New Advanced Scintillators for Gamma Ray Spectroscopy and Their Application

Sergey Svertilov[1(✉)], Vitaly V. Bogomolov[1], Anatoly Iyudin[2],
Ivan Maksimov[1], Aleksandra Markelova[2], and Ivan Yashin[2]

[1] Physics Department, Lomonosov Moscow State University, SINP, Moscow,
Russia
sis@coronas.ru
[2] Lomonosov Moscow State University, Skobeltsyn Institute of Nuclear Physics
(SINP), Moscow, Russia

Abstract. We report here results of the comparative study of different
gamma-ray spectrometers, that are using modern type scintillating crystals like
LYSO, YSO, LaBr$_3$:Ce, CeBr$_3$ and Ce:GAGG. Energy resolution of gamma-ray
detectors as derived for different combinations of scintillating crystals and
photo-sensors that were exposed to the conventional set of radioactive isotopes,
as well, as their potential use will be discussed in this paper. We also present an
example of gamma-ray spectrometer application in the long-term measurements
of flux and spectral variations of the sea level gamma-ray background radiation.
The instrument contained moderately large (80 × 80 mm) scintillating detector
with energy resolution $\sim 7\%$ at 662 keV. The data stream was recorded in
event-by-event mode with ~ 15 µs time resolution thus permitting detection of
the terrestrial gamma-ray bursts at the moment of lightning during thunder-
storms. Real time calibration of the spectrometer during the whole experiment
was performed using ^{40}K background line position (E = 1.46 MeV). This set-up
helps to exclude temperature variations of the signal in a long-term experiment.
The instrument design, as well, as the results of its long-term employment are
discussed in this chapter.

1 Introduction

Gamma-ray spectroscopy has very wide field of application in the modern fundamental
and applied nuclear physics. Gamma-ray spectroscopy is also widely used in space
research, first of all in gamma-ray astronomy, and also in high-energy atmospheric
physics. The latter means study of gamma rays, that are possibly generated in the
so-called high altitude discharges and lightning, i.e. Terrestrial Gamma Ray Flashes
(TGRF) and Thunderstorm Ground Enhancement (TGE). These observations use the
gamma-ray detectors with good energy resolution and sensitivity, which ideally should
be also able to estimate the direction of incoming quanta and locate their sources. The
most advanced modern gamma-ray instruments are based on the use of coded aperture
position sensitive detectors. Among other parameters an energy resolution is one of the
importance for selecting such detectors. It is well known, that considering energy
resolution as selection criteria among different types of gamma-ray detectors the pure

germanium semiconductor has the best energy resolution. However, application of Ge spectrometers in space research is limited due to the necessity to use cryostats for their deep cooling during operation. Luckily a substantial progress has been achieved in recent years in the development of new advanced scintillators with energy resolutions approaching those of semiconductors. For example, scintillators activated by Cerium or even made of it, such as Lanthanum and Cerium bromides ($LaBr_3$:Ce, $CeBr_3$), gallium-gadolinium garnet (Ce:GAGG) are among them. In the following, in Sect. 2 of this article we present and discuss measurements of energy resolution with $LaBr_3$:Ce, $CeBr_3$ and Ce:GAGG crystal scintillators in combination with different type photo-sensors. In Sect. 3 results of the sea level natural gamma-ray background measurements made with advanced gamma-ray spectrometer are presented.

2   Energy Resolution of $LaBr_3$:Ce, $CeBr_3$ and Ce:GAGG Crystal Scintillators in Combination with Different Type Photomultipliers, as Well as with Si-Photodiodes, to Be Used for Detection of Cosmic Gamma-Rays

2.1   Energy Resolution of Advanced Scintillators

Detector energy resolution defines accuracy with which gamma quantum energy could be measured by this detector. Formally, energy resolution value can be written as

$$R^2 = R_{stat}^2 + R_{np}^2 + R_{inh}^2 + R_{det}^2, \tag{1}$$

where, R_{stat} is the statistical error in the number of detected photons N_{dph}, R_{np} is the error caused by non-proportionality in dependence of scintillator light output on the gamma photon energy, R_{inh} is the part caused by scintillator non-uniformity and irregularities, light reflection or quantum efficiency of photo-sensor, R_{det} is the error caused by the noise and fluctuations of photo-sensor gain. The first two items in (1) are fundamental values and defined by scintillator properties.

The main parameters of some most popular inorganic scintillators are presented in Table 1.

As it could be seen from the table, Cerium bromide, Lanthanum bromide activated by Cerium and less Ce:GAGG scintillators give higher light yield and higher energy resolution in comparison with the widely used NaI(Tl) and CsI(Tl) crystals. Energy resolution measured for $YAlO_3$:Ce_3, Ce:GAGG and $LaBr_3$:0.5% Ce_3 scintillators is very similar to R_{stat} that indicates on insignificance of the remaining terms of expression (1). Situation is very different for NaI(Tl), CsI(Tl) and some other widely used scintillators.

Poor energy resolution of NaI(Tl), CsI(Tl) and other scintillators can be explained by non-proportionality of dependence of scintillator response on gamma quantum energy. This non-proportionality is directly caused by non-proportionality of dependence on electron energy. Producing of secondary energetic electrons is statistical process and it leads to fluctuations of light yield and to appearance of R_{np} term in the expression (1). Only in the case of proportionality light yield does not depend on

Table 1. Properties of considered Scintillators

Scintillating crystal	NaI(Tl) [1, 2]	CsI(Tl) [2]	LaBr$_3$: Ce [2]	Ce: GAGG [3–5]	CeBr$_3$ [6, 7]	YAlO$_3$: Ce [8]
Density, g/cm^3	3.67	4.51	5.07	6.7	5.18	5.35
Light yield, phot/MeV	40,000	54,000	68,000	57,000	68,000	14,600
Intrinsic energy resolution (662 keV)	5.9%	3.8%	1.2%	5.0	∼2.6%	?
Decay time, ns	∼200	∼2×10^3	∼16	84	∼17	∼27
Emission spectrum maximum, nm	415	550–565	360	520	380	347
Intrinsic radioactivity	No	No	Decay of ^{138}La	No	∼0.01 ph cm^{-3} s^{-1}	
Hygroscopic	Yes	No	Yes	No	Yes	Yes

secondary electron distribution. This is typical for YAlO$_3$:Ce$_3$, Ce:GAGG and LaBr$_3$: Ce$_3$ scintillators at energies about 30 keV.

Quite recently an advanced technology to produce scintillators LaBr$_3$:Ce, CeBr$_3$ and Ce:GAGG with volumes large enough to be used as effective gamma ray detectors was demonstrated. Due to their performance characteristics, like high light yield (∼60,000 phot/MeV) and sufficiently high density (5.1–6.7 g/cm^3) LaBr$_3$:Ce, CeBr$_3$ and Ce:GAGG are very suitable for use in gamma-ray spectrometers. Short decay time (∼20 ns) makes their application optimal in the case of necessity to have high accuracy timing measurements with integration time less than 0.1 mcs, as well, as detection of high fluxes, i.e. to have the high bandwidth of measurement tract.

Energy resolution of LaBr$_3$:Ce, CeBr$_3$ and Ce:GAGG scintillators was measured for number of laboratory samples of corresponding crystals with relatively small sizes. The results of these measurements are presented below.

2.2 Results of Energy Resolution of LaBr$_3$:Ce, CeBr$_3$ and Ce:GAGG Crystal Measurements

The following main factors, that usually influence, or contribute to the measured energy resolution, were taken into account during measurements:

- intrinsic resolution of scintillator itself (defined as non-proportionality between the light yield and the energy deposited in the crystal);
- (non)uniformity of the light-gathering and photo-cathode quantum efficiency (corresponding dispersion depends strongly on geometry and optical properties of the crystal);
- Poisson fluctuations of the photo-electrons number that is defined by the energy release in the crystal, light-gathering efficiency and photo-cathode quantum efficiency;
- Electronics noise and photo-sensor gain fluctuations.

As it was mentioned above photo-electron statistics gives the main input in the energy resolution of LaBr$_3$:Ce, CeBr$_3$ and Ce:GAGG scintillator crystals of small volume.

Measurements were made for different crystals and different photo-sensors with the number of radioactive isotopes. Energy resolution was measured for the following crystals:

1. LaBr$_3$:Ce with sizes Ø15 × 18 mm;
2. LaBr$_3$:Ce with sizes Ø5 × 15 mm;
3. Ce Br$_3$ with sizes Ø5 × 15 mm;
4. Ce:GAGG with sizes 10 × 10 × 30 mm.

Scintillator crystals NaI(Tl) Ø10 × 10 mm and YSO 10 × 10 × 30 mm were also used as control samples. LaBr$_3$:Ce and CeBr$_3$ samples used in this work were produced in Solid State Physics Institute of Russian Academy of Science (Chernogolovka, Russia).

Photo-multiplier tubes (PMT) Hamamatsu R2248 and Uspekh as well as avalanche photo diode (APD) Hamamatsu S8664-1010 and silicon photomultiplier (SiPM) SensL matrix ArrayB-30035-144P-PCB with AIT preamplifiers were used as photo-sensors. R2248 is head-on PMT with the quadratic photocathode of 1 cm^2 size, that allows effective collection of light from crystals with the same quadratic shape 1 cm^2 cross-section. The quadratic shape of this PMT promotes the densest possible packing of position sensitive detector pixels.

Radioactive sources and photons energies that were used in our measurements are listed in Table 2.

Table 2. Isotopes and photon energies used in our measurements

Energy	Isotope	Energy	Isotope
26.34	Am241	511	Na22
30.9	Ba133	569.7	Bi207
32	Cs137	661.65	Cs137
40	Eu152	778.9	Eu152
59.54	Am241	867.38	Eu152
75	Bi207	964.1	Eu152
81	Ba133	1063.66	Bi207
101	Am241	1173.2	Co60
121.78	Eu152	1274.5	Na22
244.7	Eu152	1332.5	Co60
344.28	Eu152	1408	Eu152
356	Ba133	1770	Bi207

Radioactive source with $\sim 10^5$ Bk activity was placed on a small ~ 5 cm distance from the detector end. The amplitude spectra were measured for about 5×10^5 events in the tested scintillator crystal. The schematic diagram of the experimental setup is

shown in Fig. 1 (the position of the analogous switches corresponds to the initial state). The setup comprises the detector assembly composed of a scintillation crystal sample with a photo-sensor, that were placed in a light-tight box (not shown in the figure), and the electronics board. This setup also includes a personal computer used to read out and to process signals from the output registers, as well, as Tektronix TDS3012B oscilloscope and Tektronix AFG3102 arbitrary function generator, that were used to adjust the electronics parameters. The crystal sample under investigation was placed approximately at the centre of the PMT entrance window. Optical contact between the entrance windows of the crystal packing and the PMT was made with the use of a special glycerol based lubricant.
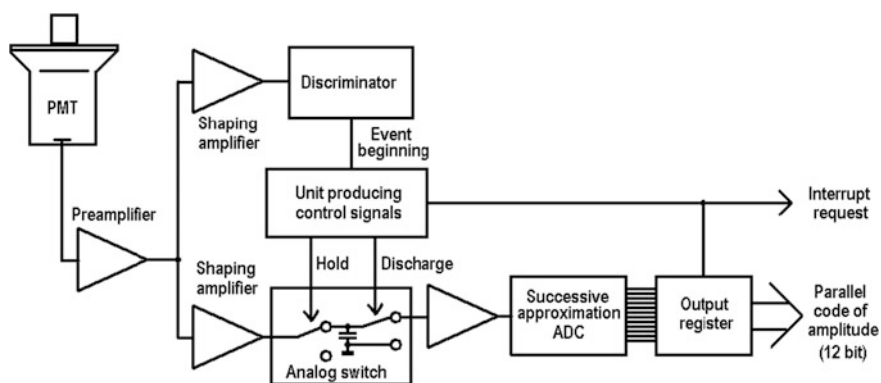
Fig. 1 The wire diagram of energy spectra measurement unit

The electronic boards contained the PMT high-voltage power supply based on EMCO CA20 N and integrated circuits used to perform the measurements. All signals from the photo-sensor anode were consequently fed into the AD8014 preamplifier and then to AD8014 shaping amplifiers, for the later amplitude measurements and trigger generation. The trigger was generated using an amplitude discriminator based on an AD8561 comparator when the PMT output signal exceeded a certain "background" level corresponding to $\sim 10\_keV$ energy deposit in the scintillator crystal. The trigger signal corresponds to the beginning of a detected event, and its leading edge triggers the control signal generating circuit that produces a rectangular Transistor–Transistor Logic (TTL) pulse with a duration of 0.5 mcs, that is controlling the analogous switch and the output register. The analogous switch was used to convert the rapidly changing output signal from the PMT into a constant voltage level suitable for analysis of its value with a successive approximation analogue to digital converter (ADC). In the initial state, both arms of the analogous switch were in the closed position shown in the Fig. 1. In this state, the signal was integrated with a characteristic time of ~ 150 ns. The first arm of the switch was opened by the Storage signal from the control signal circuit. As a result, the charge accumulated from the beginning of the pulse was still

stored in the capacitor disconnected from the input. Switching happened within a time interval of ~ 50 ns, thus ensuring complete light collection in view of the scintillator decay time (~ 20 ns).

The voltage level formed by integration was fed to the AD7492 ADC via an auxiliary isolating amplifier. The integrating capacitor was short circuited to ground by the Discharge signal arriving from the control signal circuit after the expiry of the conversion time (~ 1 mcs), which ensured its fast discharge and its readiness to convert the next signal. As a result, both arms of the analogous switch returned thereby to the initial position within a time interval of ~ 1 mcs. The amplitude code written in the ADC bits is stored in the output register and rewritten by the Interrupt Request signal into the memory of the personal computer over a 12 bit parallel interface. The ADLINK PCI-7396 parallel input/output board was used for this purpose.

The energy resolution of the scintillators crystals was also measured using standard signal converter modules of NIM crate. The measurements were made using the H5783-03 PMT assembly that also contains the voltage divider and the high voltage converter, for different values of the control voltage determining the PMT mode. The PMT signals were fed first into Ortec 450 shaping amplifier with the integration time of 100 ns, and then into MCA-3 multichannel analyser (the PCI modification). An auxiliary Canberra 2037A discriminator was used to eliminate detection of spurious signals that appeared on the tails of pulses with too high amplitudes and overloaded the electronics. After logic shaping (Canberra 2055), the signal from this amplifier was fed into the MCA-3 control input for use in the anticoincidence mode. The values of the high voltage applied to the photo-sensor were selected so that the signal to noise (SNR) ratio was optimized and signal amplitude measuring section exhibited the maximum linearity in the range of measurable gamma quantum energies. Adjustable preamplifier gain (K_{pa}) allowed regulation of the amplitude range of the electronics channel in order to select the desired part of the measured energy spectrum.

Examples of energy resolution measurements with the use of advanced scintillator crystals are presented below.

Energy spectrum obtained for $\varnothing$15 mm×18 mm $LaBr_3$:Ce crystal irradiated by ^{137}Cs source (line 662 keV) and viewed by PMT Uspekh is presented in Fig. 2. PMT Uspekh was used as photo-sensor with optic window covered the UV band. As it could be seen from the figure, energy resolution at 662 keV (ADC channel 3250) was 3.2% (FWHM).

Energy resolution measured with other radioactive sources with lines corresponded different energies (3.6% for ^{22}Na, annihilation line 511 keV, 6.8% for ^{57}Co, 122 keV) indicates on good linearity of dependence of detector output signal amplitude on gamma quantum energy [6]. Measured energy resolution of $LaBr_3$:Ce crystals of small volume (~ 1 cm^3) at room temperature is quite compatible with energy resolution of semiconductor detectors CdTe and CdZnTe with similar sizes obtained for room temperatures also.

Energy resolution was also measured for $CeBr_3$ crystal of small volume $\varnothing 5 \times 15$ mm. The example of energy spectrum of Bi-207 is presented at Fig. 3. The energy dependence of the energy resolution obtained with different isotopes demonstrates that in all energy range from about 30 keV up to ~ 2 MeV $CeBr_3$ scintillator
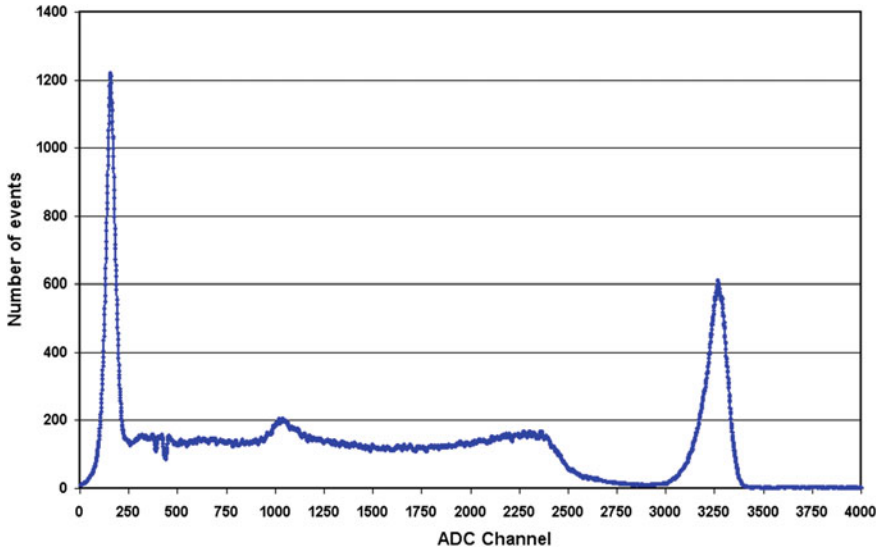
Fig. 2 Energy spectrum of ^{137}Cs source of 662 keV photons obtained with ∅15 mm × 18 mm LaBr$_3$:Ce crystal and PMT Uspekh

has energy resolution a little worse but quite compatible with LaBr$_3$:Ce. Taking into account the absence of intrinsic radioactivity and, hence, the lower intrinsic background [9], it allows us conclude that CeBr$_3$ is very perspective for using in gamma spectroscopy.
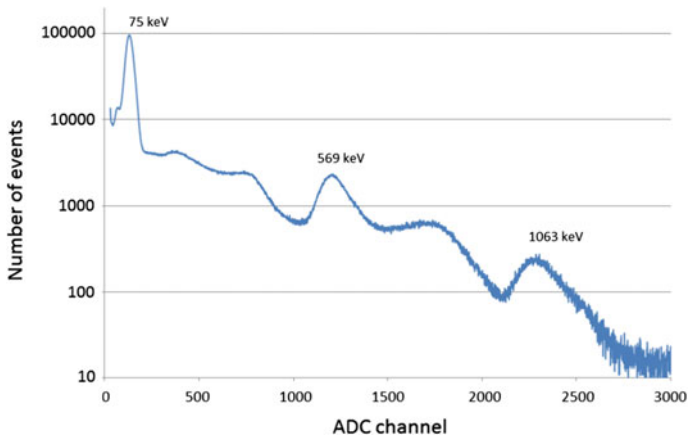

Fig. 3 Energy spectrum of Bi-207 measured with CeBr3 ∅5 × 15 mm

Energy spectra of several gamma-ray sources were also measured for 10×10 30 mm Ce:GAGG sample and for control scintillators NaI(Tl) $\varnothing 10 \times 10$ mm and YSO $10 \times 10 \times 30$. Measurements were made with different types of photo-sensors, such as PMT (Hamamatsu R2248), APD (Hamamatsu S8664-1010) and SiPM matrix (SensL ArrayB-30035-144P-PCB). The results of measurements with R2248 PMT are presented in Fig. 4.
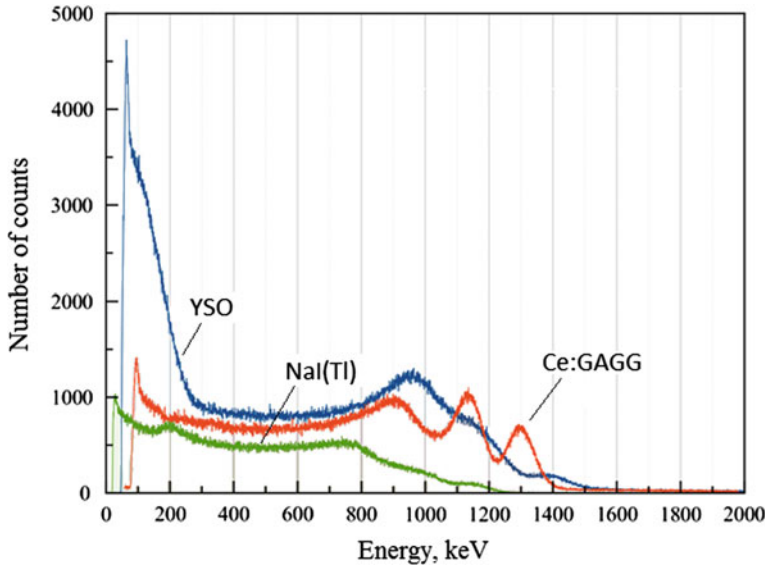

Fig. 4 Energy spectra from Co-60 source measured by PMT R2248 with different small size scintillator crystals

It is following from the Fig. 4 that neither NaI(Tl) nor YSO resolve the ^{60}Co lines (1.17, 1.33 MeV), while the are resolved clearly by Ce:GAGG scintillator. This means that it has sufficiently better energy resolution as well as stop factor. The other example of Ce:GAGG advantages is given by Fig. 5, in which there are presented the energy spectra measured with different isotopes for NaI(Tl) and Ce:GAGG scintillators viewed by APD. As it could be seen from the figure, all peaks from isotope gamma ray lines are revealed more clear with Ce:GAGG, which peaks are also more narrow that indicates on higher energy resolution.

Energy resolution was also measured for Ce:GAGG crystal viewed by ArrayB-30035-144P-PCB SiPM (12×12 pixels) matrix. The example of energy spectrum obtained with [152]Eu isotope is presented in Fig. 6.

As it is shown in the Fig. 6, all [152]Eu lines, like 121.78, 244.7, 344.28, 778.9, 867.38, 964.1, and 1408 keV are revealed clearly. Energy resolution of Ce:GAGG crystal at different energies is compared to that of NaI(Tl) crystal in Fig. 7.
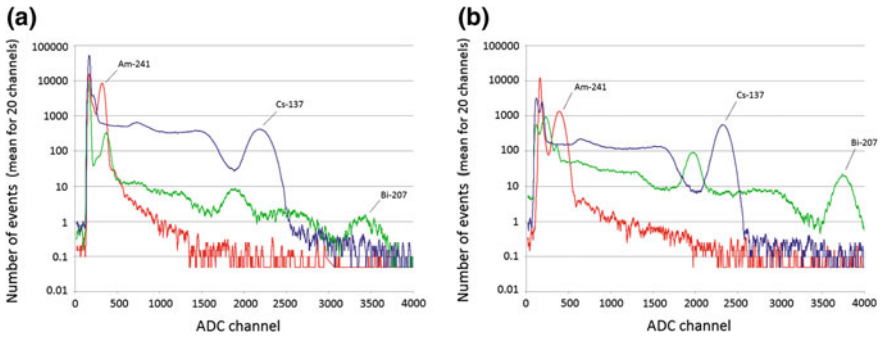
Fig. 5 **a** Energy spectra of different gamma ray sources measured by APD photo sensor and $\varnothing 10 \times 10$ mm NaI(Tl) crystal at APD. **b** Energy spectra of different gamma ray sources measured by APD photo sensor and $10 \times 10 \times 30$ mm Ce:GAGG crystal at APD
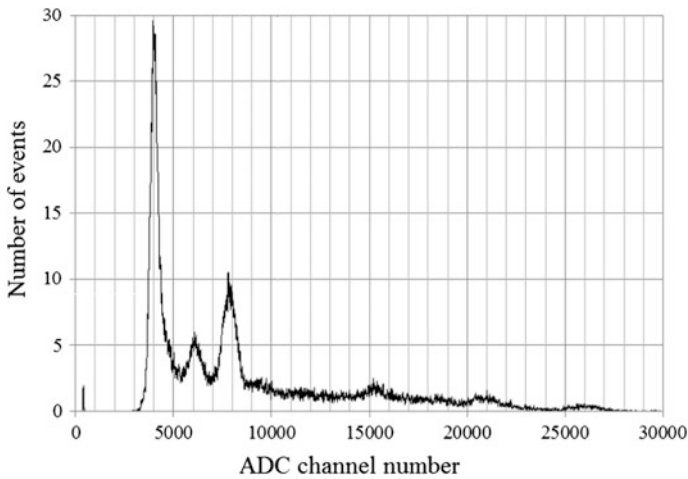

Fig. 6 Summary spectrum obtained with Ce:GAGG crystal and [152]Eu source

As it could be seen from the figure, in all energy range Ce:GAGG crystal demonstrates the better energy resolution than NAI(Tl) crystal. Thus, we may conclude that comparing energy resolution of tested crystals YSO, LaBr₃:Ce, CeBr₃ and Ce:GAGG, only the latter demonstrates the best energy resolution with the use of different type photo-sensors such as PMT, APD, SiPM. This indicates that Ce:GAGG crystal has an excellent perspective for application in gamma ray spectroscopy.
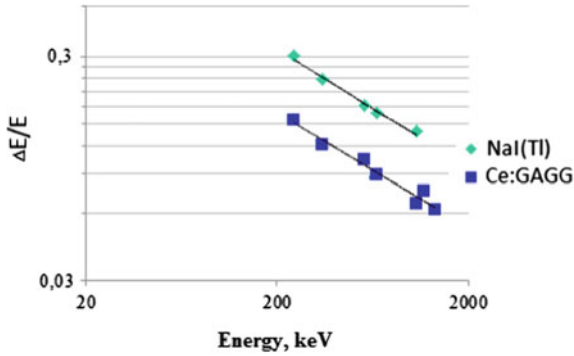
Fig. 7 Dependence of ΔE/E on energy for NaI(Tl) and Ce:GAGG crystals

3 Scintillating Spectrometer for Long-Term Study of the Sea Level Gamma-Ray Background Variations Caused by Changes of Concentration of Radioactive Isotopes and Particle Acceleration During Thunderstorms

3.1 Advanced Position Sensitive Gamma Spectrometer for Gamma Ray Spectroscopy in Space and Ground Experiments

The advanced position sensitive gamma ray spectrometer based on the Ce:CAGG scintillator pixels was elaborated for space and ground experiments. This instrument is also able to detect neutrons with energies from about 1 to 100 MeV. The main application of the instrument is a study of atmospheric gamma rays and possibly neutrons that are generated during thunderstorms. Instrument also can be used for the purposes of gamma ray astronomy and geoscience research, i.e. for detection of cosmic gamma ray bursts, gamma rays from solar flares, to study terrestrial gamma ray flashes from space, and also for the study of neutron fluxes of solar, atmospheric and terrestrial origin. The design of analog and digital electronics of such instrument has to foresee the stable long-term performance capability with the microsecond time resolution, as well, as the time reference to UTC with microsecond accuracy. The results of atmospheric gamma ray flux measurements by the prototype of such instrument based on NaI(Tl) scintillator are presented in Sect. 3.2.

The advanced instrument is based on the use of the SiPM matrixes, of pixelated Ce: GAGG, and of plastic scintillator fibers arranged in a charged particle track recording spectrometer, which allows to determine the energy and direction of the detected gamma quanta in the energy range from 10 keV up to a few MeV and neutrons with energies from 1 to 100 MeV. Electronic triggers are realized by the program that includes the possibility of detection of various types of particles and of gamma photons. The principle of gamma photon detection is determined by two or three Compton interactions in the volume of a tracker, while detection of fast neutrons is performed in the mode of elastic neutron scattering on hydrogen nuclei in the scintillation fiber. The general view of such instrument is presented in the Fig. 8. The hodoscope tracker unit

is placed in the upper part of the instrument. It is the assembly of scintillator fibers alternatively oriented along axes perpendicular to the instrument symmetry axes, that are viewed by SiPM matrixes. Small fiber thickness (1.5 mm) provides high spatial resolution for gamma photons and neutrons detection. At the bottom of the tracker the calorimeter assembly is placed, that consists of a set of Ce:GAGG crystals of $10 \times 10 \times 30$ mm^3 size, intended for the detection of gamma rays scattered ones, or twice in the hodoscope. The thickness of these detectors enables to detect with high efficiency the gamma quanta with energies up to several MeV. As it was shown previously, the energy resolution $\sim 4\%$ can be achieved for photons with an energy of about 1 MeV absorbed by the Ce:GAGG scintillators crystal of $10 \times 10 \times 30$ mm^3 size (see Fig. 7).
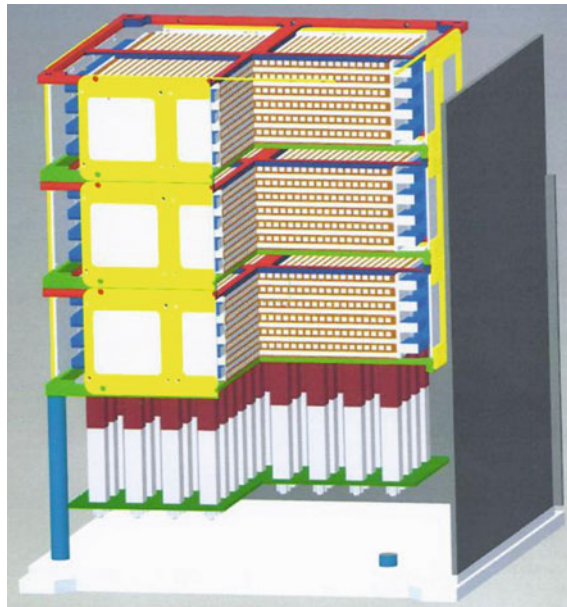

Fig. 8 The general view of the imaging gamma-ray and neutron scintillating spectrometer

3.2 Scintillating Spectrometer for Measurements of Atmospheric Gamma Rays

The prototype of scintillator gamma ray spectrometer based on NaI(Tl) crystal was used for the study of atmospheric gamma ray fluxes. There are a few cases reported in the past when an excess of gamma ray flux, additional to constant background, was registered during thunderstorms. The detected gammas were mostly described as the bremsstrahlung of electrons accelerated in high electric fields presumably generated under thunderstorm conditions. Spectra of those additional gamma ray fluxes can be described in boundaries of the relativistic runaway electrons avalanche model [10, 11].

Excesses of gamma ray fluxes connected with atmospheric electricity were observed in wide range of time scale including fast flashes in sub-millisecond range (so-called Terrestrial gamma flashes (TGFs) [12], as well, as comparatively slow phenomena like so-called Thunderstorm ground enhancements (TGEs), lasting up to several hours [13, 14]. TGFs are usually studied by the satellite experiments with gamma spectrometers working in "classical" energy range from several hundreds of keV to several MeV, but there are also several observations of TGFs from lightning at the ground level [15]. It must be noted that the radiation from TGFs has hard spectra with energies extended up to several tens of MeV. Other fast phenomena observed in the past few years is the termination of TGE at the moment of lightning [16]. The flux of hard radiation drops to pre-TGE level during several seconds or even less.

To perform observations at the low energy range of gamma ray emission at the ground level, or at low altitudes in atmosphere, well-calibrated detectors of sufficient area based on scintillator crystals are needed. It is very important because a large part of gamma-ray flux variations in the range E < 2.5 MeV can be explained by changes of Rn-222 concentration connected with rainfalls during thunderstorms [17]. Energy resolution of such detectors must be suitable for detection of discrete gamma-ray lines produced by the decay of radioactive isotopes in order to control Rn-222 and its daughter concentration, and to make real time on-line calibration of the spectrometer during the experiment with background lines. The instrument has to have stable (up to $\sim 1\%$) performance characteristics for long-duration measurements, as well, as sufficiently good time resolution to detect possible short flashes of gamma ray emission.

Several instruments used in this work for atmospheric transient events study were gamma-ray spectrometers based on the well studied non-organic scintillators, like NaI (Tl) or CsI(Tl). Electronic circuits developed for use in these spectrometers can work with the single-crystal detector, as well, as with the multilayer detector, that allows determination of the crystal type in which interaction took place via the pulse-shape analysis. Such kind of analysis allows to remove imitations of gamma-events by the lightning following pulses of electrons. One can read the detailed description of the instrument design in the proceedings of TEPA-2015 conference [17].

The structural diagram of electronics of gamma-spectrometer is presented in Fig. 9. It consists of "Power supplying unit" providing high voltage (~ 1000 V) for PMT and low voltage for analog and digital electronics, "Event" card containing analog electronics for event triggering and pulse-shape analysis, and "Data collecting card" based on the board STM32F4DISCOVERY with Cortex M4 microcontroller. GPS module with PPS is used for exact timing providing synchronization of gamma-ray spectrometer readings with the world time with accuracy ~ 10 µs. The output data are read-out to SD card with a one second cycle. The data are recorded in the event-by-event mode and contain detailed time and amplitude information for each recorded interaction in the detector.

Detailed spectral information that is contained in the data allows one to do real-time calibration with the use of background gamma-ray lines observed during the measurements. The algorithm of data processing derives the position of the detected 1.46 MeV background gamma-ray line of K-40. The actual instrumental channel of K-40 line peak position is calculated and stored in the memory every 300 s. The energy of each detected gamma-quantum then calculated in units of energy using
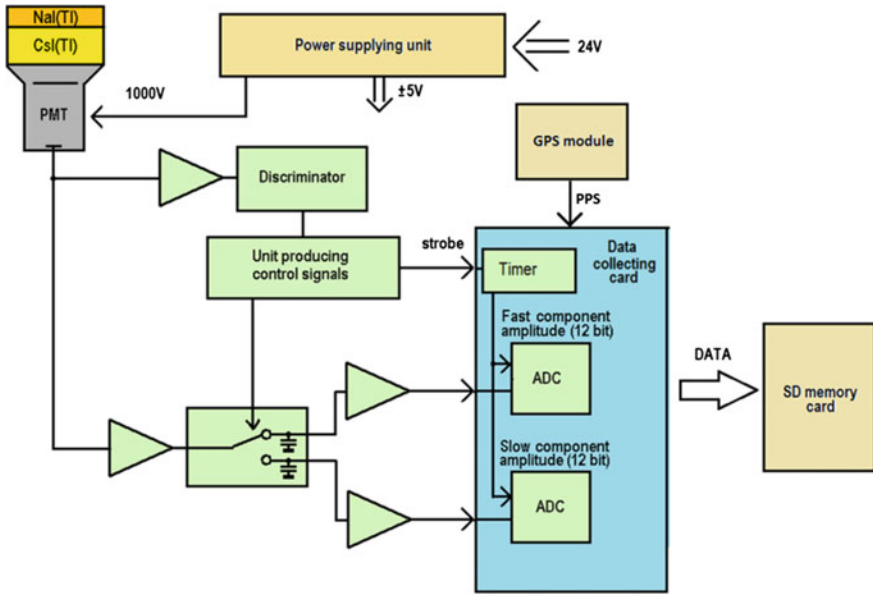
Fig. 9 Structural diagram of scintillator gamma-ray spectrometer

corresponding linear formula. Such procedure allows minimize effect of the electronics gain variations caused by the temperature drift of the detector characteristics. For the long-lasting observation series such real-time calibration capability is very important, because day and night temperature can differ by more than 20°. The temperature measurements taken during sunny day and/or thunderstorm weather can also greatly differ. The position of K-40 gamma-ray line measured during one-week measurements session is presented by Fig. 10 demonstrate ∼10% variations.

A few different gamma-ray spectrometers were produced by us for measurements of natural gamma ray background variations. One of them (see photo at Fig. 11) was used for the study of TGEs and the search for gamma-flashes from lightning in Moscow region. It has detector based on 80 × 80 mm CsI(Tl) crystal coupled with Hammamatsu R1307 PMT. Results of the experiment with this spectrometer in low energies (<3000 keV) in 2015 were presented and discussed at TEPA-2015 proceedings [17]. For measurements during 2016, somewhere in May, 2016 the energy range of the spectrometer was extended up to 6000 keV, and GPS module was added to the set up. Therefore during summer 2016 measurement session it was possible to record gamma-ray background spectra in 30–6000 keV energy range with the energy resolution of 7.2% at 662 keV.

Spectrometers used for monitoring of gamma-ray background were calibrated with a number of radioactive sources. Some of the energy spectra obtained during calibration sessions are presented in Fig. 12. One can easily recognize well known peak of 662 keV line from Cs-137 decay, and a set of background lines that are corresponding to the most intense radiation of naturally occurring isotopes of K-40, Tl-208 (daughter of Th-232) and Bi-214 (daughter of Rn-222).
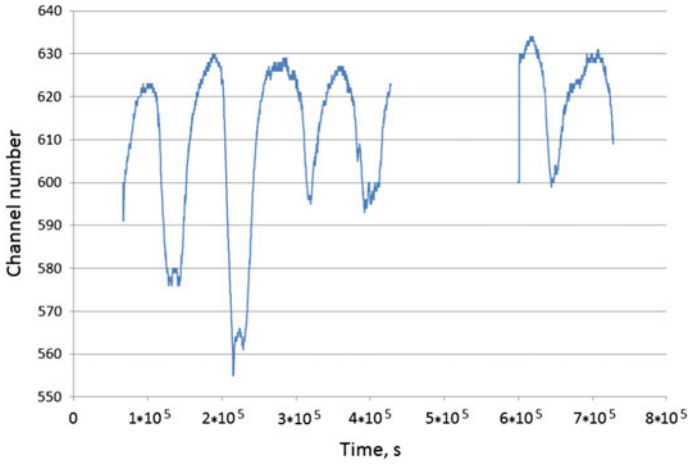
Fig. 10 Time variations of the position of K-40 gamma-ray line measured during one session of measurements

Fig. 11 Photo of the gamma-spectrometer used for the study of TGEs and for the search for gamma-flashes from lightning in Moscow region. GPS sensor is placed on the detectors head

3.3   Thunderstorm Ground Enhancements (TGEs) Measurements

The measurements in Moscow region were made in two places, both are ~ 50 km North and North-west from Moscow. During measurements session of a summer 2016 there were several thunderstorms for which it was possible to compare temporal and
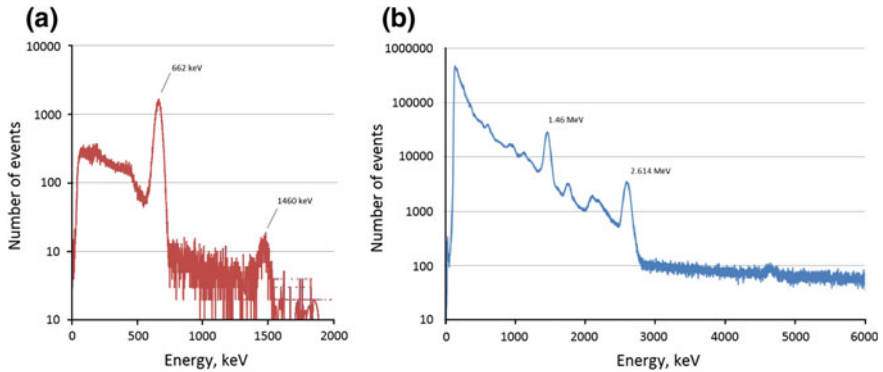
Fig. 12 Spectrum of Cs-137 (**a**) and background spectrum (**b**) obtained with the 80 mm diameter CsI(Tl) detector in Moscow region. Lines at 1.46 and 2.614 MeV correspond to the naturally occurring isotopes K-40 and Tl-208

spectral characteristics of TGEs of gamma radiation, that were caused by the same thunderstorm in two neighboring regions. The behavior of the hard gamma radiation with energy of E > 3 MeV is of special interest, because at those energies there are no gamma-quanta from Radon daughters to be expected.

The spectrogram and the time sequence of gamma-ray fluxes measured from 13.06.2016 to 17.06.2016 are presented at Fig. 13. A quite intense thunderstorm has occurred during 16.06.2016. TGE was observed by our detectors from ∼16 h to ∼20 h UTC. It can be seen on the spectrogram that intense additional radiation at 609-keV gamma-ray line of Bi-214 has appeared during this thunderstorm. It leads us to conclude, that in this case changes of Rn-222 concentration that are caused by the rain-shower are responsible for the observed TGE in the low energy range of observed gamma radiation. One can also see, that no changes of the gamma-ray flux were observed in the 3200–6000 keV high-energy channel.

One more TGE was observed on 18.07.2016. Its time profile in different energy channels is presented at Fig. 14. One can see the increase of gamma-radiation for more than 3 h. In most of low-energy channels the amplitude of this TGE reached 100%. The energy spectra obtained for ∼10,000 s during the flux maximum and during the quite period before TGE are presented on the top panel of Fig. 15. Bottom panel of Fig. 15 shows TGE spectrum after subtraction of the natural background. One can observe many of Bi-214 gamma-ray lines and conclude that most of low energy radiation was connected with the Rn-222 decay chain.

The excess emission for time periods with detected TGE if compared to the pure background periods is best observed in the hardest energy channel, and is <1.4%, that corresponds to significance of 1.8 sigma. The upper limit (3-sigma level) of TGE gamma-ray flux in 3200–6000 keV energy range is 2.4×10^{-4} cm^{-2} s^{-1}.

One can conclude that most of energy spectra obtained in 20–3000 keV energy range during thunderstorms in Moscow region show the presence of gamma-ray lines associated with Rn-222 and daughters. The measurements made on rainy days without thunderstorm demonstrate similar variations of Rn-222 concentration. The variations of
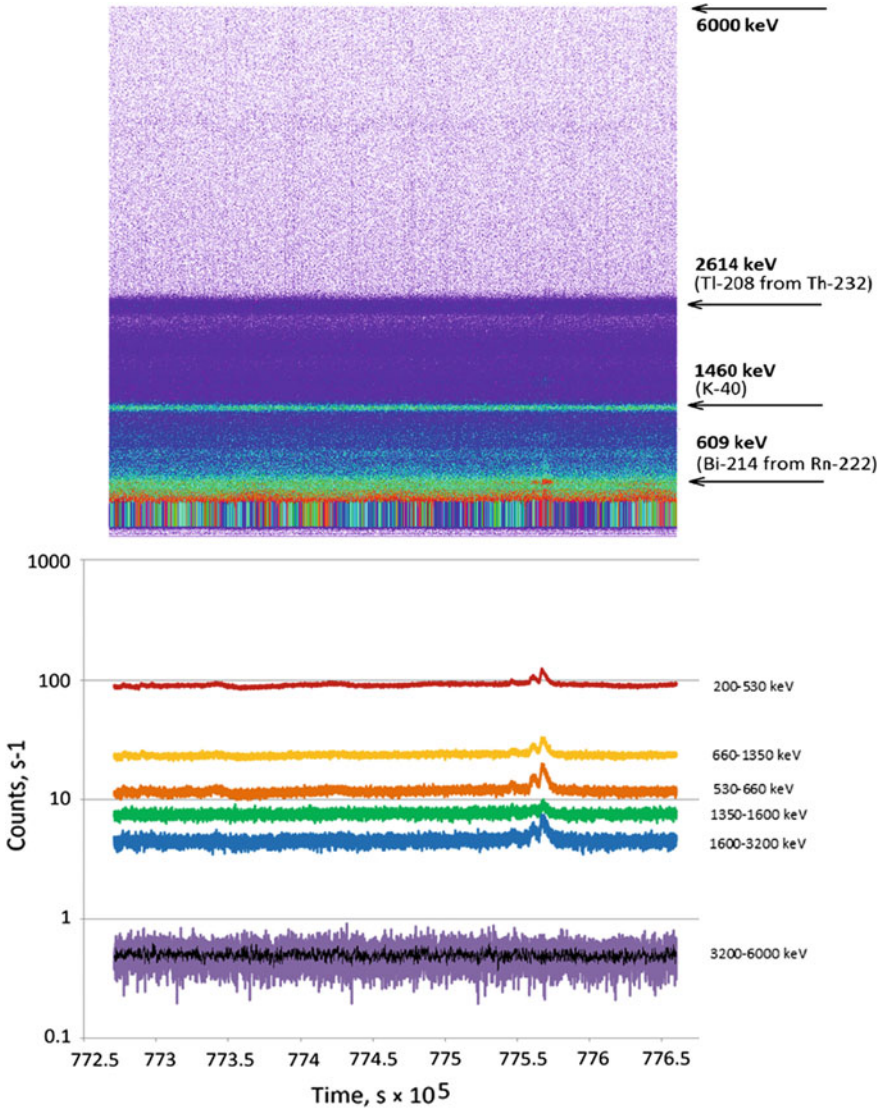
Fig. 13 Spectrogram (top panel) and time profile in several energy channels (bottom panel) of gamma radiation measured during thunderstorm in Moscow region

Rn-222 gamma-ray background are much greater than ones expected from bremsstrahlung from the electrons accelerated in thunderclouds in the same energy range. However variations of natural radioactivity do not influence on gamma-spectra in the high energies above 3 MeV. A number of thunderstorms were observed in Moscow region during measurements session of 2016. All of them do not show TGE radiation above 3.2 MeV. Upper limit of TGE flux in 3.2–6 MeV energy range for
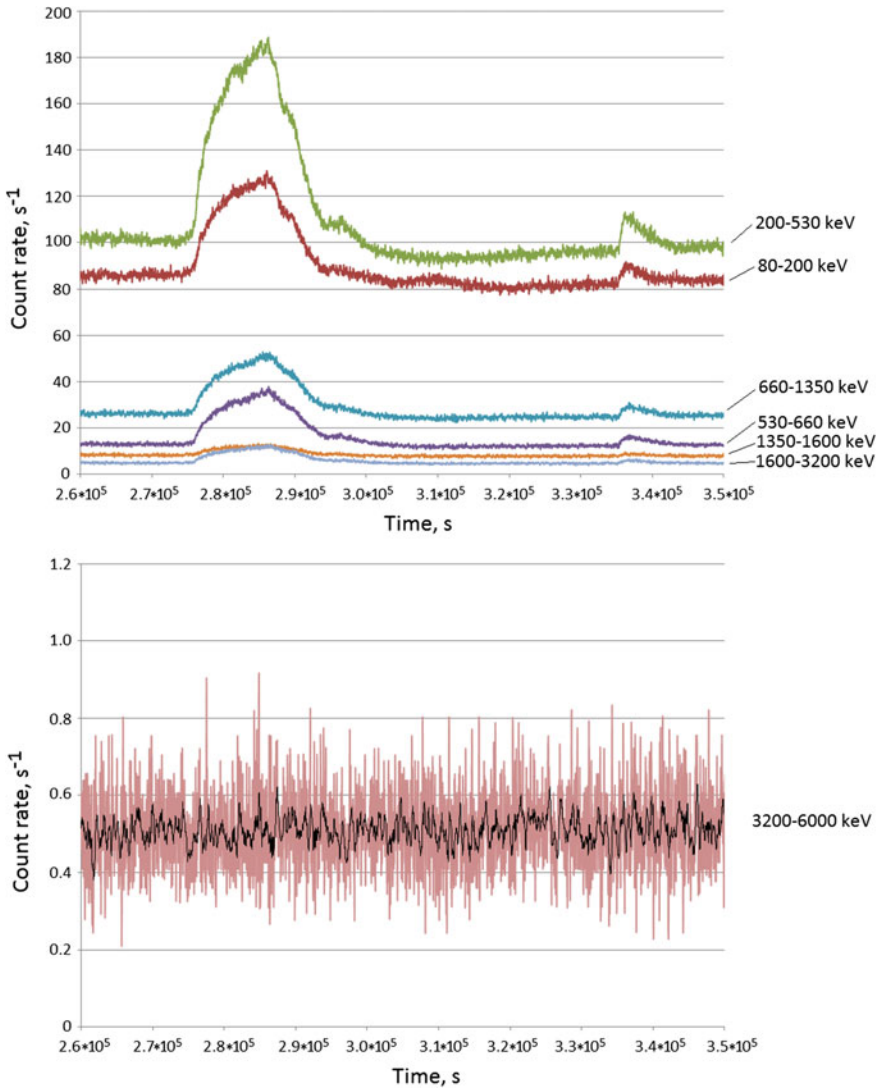
Fig. 14 Time profile of TGE observed on July 18, 2016

measurements in the Moscow region is of the same order of magnitude as the flux measured at Aragatz station [14]. These results do not contradict each other, though, because the distances to the thunderstorm clouds observed during measurements in Moscow region were several times larger of those observed in the Aragatz station region.
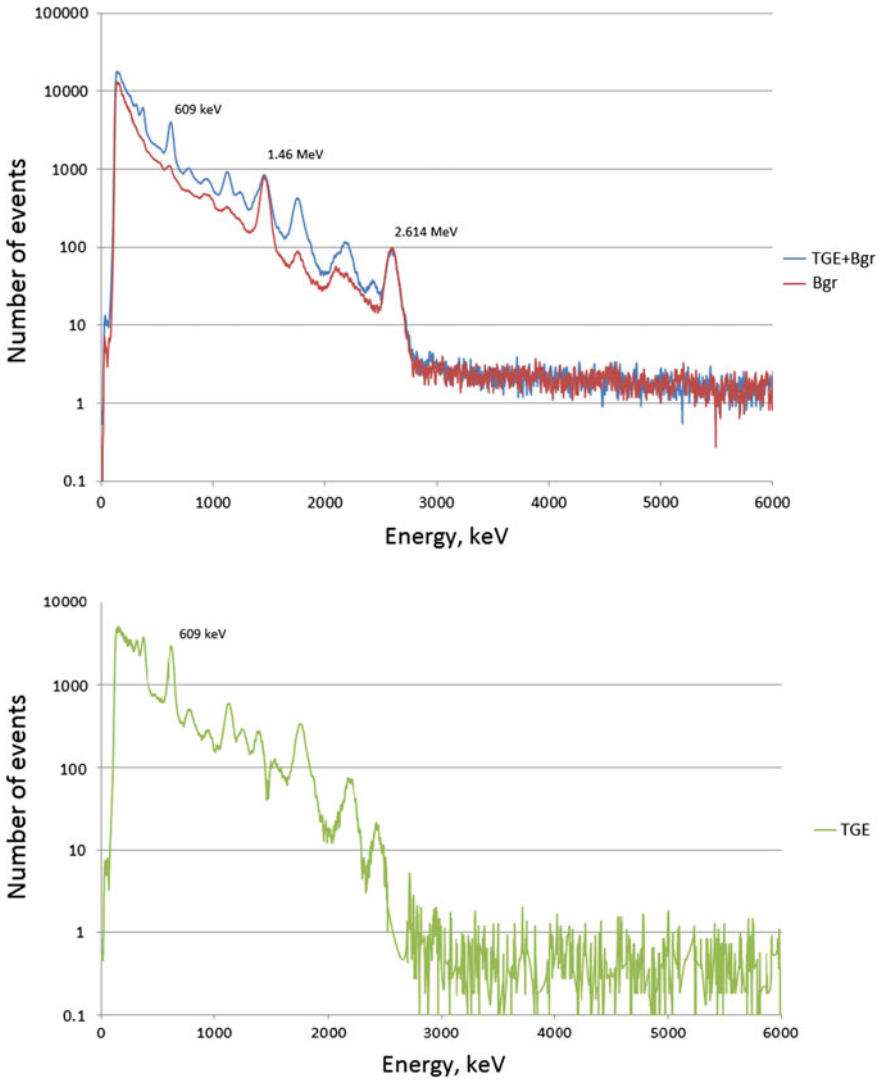
Fig. 15 Energy spectra obtained during the period of July 18, 2016 thunderstorm in Moscow region

References

1. Yu.A Tsirlin, M.E. Globus, E.P. Sysoeva, *Optimizatsyja detektirovanija gamma-izluchenija scintillatsyonnymi kristallami* (Energoatomizdat, Optimization of the detection of gamma-radiation by scintillator crystals) Moscow, 1991)
2. B. Pirard, C. d'Uston, S. Maurice, O. Gasnault, Performance limits of new generation scintillators for planetary gamma-ray spectroscopy. Lunar Planet Sci. **36**, 1–2 (2005)

3. W. Drozdowski, K. Brylew, M.E. Witkowski, A.J. Wojtowicz, P. Solarz, K. Kamada, A. Yoshikawa, Opt. Mater. **36**, 1665–1669 (2014)
4. Kei Kamada, Takayuki Yanagida, Takanori Endo et al., J. Cryst. Growth **352**, 88–90 (2012)
5. J. Iwanowska, L. Swiderski, T. Szczesniak et al., NIMA **712**, 34–40 (2013)
6. J. Glodo, A. Kuhn, W.M. Higgins et al., CeBr$_3$ for time-of-flight PET, in *2006 IEEE NSS Conference Record*, 1570–1573 (2006)
7. R. Billnert, S. Oberstedt, E. Andreotti, M. Hult, G. Marissens, A. Oberstedt, New information on the characteristics of 1 in × 1 in. ceriumbromide scintillation detectors, NIM A **647**, 94–99 (2011)
8. M.V. Korzhik, A.A. Fedorov, Scintillatsyonnye kristally na osnove redkozemelnykh aliuminievyh perovskitov (Scintillation crystals on the basis of rare-Earth aluminium perovskites), in V.G. Bardyshevsky (ed) Fundamentalnye i prikladnye fizicheskie issledovanija 1986–2001 (Fundamental and applied physical research in 1986–2001), Minsk, BGU, Institute of Nuclear Problems, 396–421 (2001)
9. A.F. Iyudin, V.V. Bogomolov, S.I. Svertilov et al., Peculiarities of intrinsic background in LaBr 3: Ce and CeBr3 scintillating crystals. Instr. Exp. Tech. **52**(6), 774–781 (2009)
10. A.V. Gurevich, G.M. Milikh, R. Roussel-Dupre, Runaway electron mechanism of air breakdown and preconditioning during a thunderstorm. Phys. Lett. A **165**, 463–468 (1992)
11. J.R. Dwyer, D.M. Smith, S.A. Cummer, High-energy atmospheric physics: terrestrial gamma-ray flashes and related phenomena. Space Sci. Rev. **173**, 133–196 (2012). doi:10.1007/s11214-012-9894-0
12. M.S. Briggs, S. Xiong, V. Connaughton et al., Terrestrial gamma-ray flashes in the Fermi era: improved observations and analysis methods. J. Geophys. Res. Space Phys. **118**, 3805–3830 (2013). doi:10.1002/jgra.50205
13. A. Chilingarian, Thunderstorm ground enhancements—model and relation to lightning flashes. J. Atmos. Solar Terr. Phys. **107**, 68–76 (2014)
14. A. Chilingarian, G. Hovsepyan, E. Mnatsakanyan, Mount Aragats as a stable electron accelerator for atmospheric High-energy physics research, in Proceeding of International Symposium TEPA-2015, (Nor-Amberd, Armenia, 2015a) pp. 2–9
15. J.R. Dwyer, M.M. Schaal, E. Cramer et al., Observation of a gamma-ray flash at ground level in association with a cloud-to-ground lightning return stroke. J. Geophys. Res. **117**, A10303 (2012). doi:10.1029/2012JA017810
16. A. Chilingarian, G. Hovsepyan, G. Khanikyanc et al, Thunderstorm ground enhancements (TGEs) abruptly terminated by negative cloud-to-ground lightning, in Proceeding of International Symposium TEPA-2015, (Nor-Amberd, Armenia, 2015b) pp. 71–78
17. V.V. Bogomolov, S.I. Svertilov, I.A. Maximov et al, Study of TGEs and gamma-flashes from thunderstorms in 20–3000 keV energy range with SINP MSU Gamma-Ray spectrometers, in Proceedings of International Symposium TEPA-2015, (Nor-Amberd, Armenia, 2015) pp. 41-46